Force line breaks with

One-dimensional particle simulation of the filamentation instability: electrostatic field driven by the magnetic pressure gradient force

M. E. Dieckmann, I. Kourakis, and M. Borghesi

Centre for Plasma Physics, Queen's University Belfast, Belfast BT7 1NN, U K

G. Rowlands

Physics Department, Warwick University, Coventry CV4 7AL, U K

(Dated: June 10, 2009)

Abstract

Two counter-propagating cool and equally dense electron beams are modelled with particle-in-cell (PIC) simulations. The electron beam filamentation instability is examined in one spatial dimension, which is an approximation for a quasi-planar filament boundary. It is confirmed, that the force on the electrons imposed by the electrostatic field, which develops during the nonlinear stage of the instability, oscillates around a mean value that equals the magnetic pressure gradient force. The forces acting on the electrons due to the electrostatic and the magnetic field have a similar strength. The electrostatic field reduces the confining force close to the stable equilibrium of each filament and increases it farther away, limiting the peak density. The confining time-averaged total potential permits an overlap of current filaments with an opposite flow direction.

PACS numbers: 52.38.Hb,52.35.Qz,52.65.Rr

The electron beam filamentation instability (FI) generates magnetic fields in energetic astrophysical[1, 2] and solar flare plasmas[3] and in laser plasma interactions[4, 5], if the beam speeds $|\mathbf{v}_b|$ are comparable to c and if the densities of the counterstreaming beams are similar[6]. It has been investigated with one-dimensional (1D) PIC and Vlasov simulations[7, 8] and with two-dimensional (2D) PIC simulations[9, 10]. The counterstreaming electron beam instability has also been examined with a 3D PIC simulation[11]. Mobile ions and a guiding magnetic field have been taken into account[7, 10, 12] and statistical properties of the FI have been obtained[13, 14, 15].

The FI triggers the growth of waves with the wavevectors $\mathbf{k} \perp \mathbf{v}_b$ over a wide band of $k = |\mathbf{k}|$, where the wavenumbers k are of the order of the inverse electron skin depth. The electrons are deflected by the magnetic field perturbation, and electrons moving in opposite directions separate in space. The net current of these flow channels amplifies the initial perturbation and, thus, the tendency to form current channels. The magnetic field amplitude grows exponentially and it saturates by the magnetic trapping of electrons[8]. The FI can also couple nonlinearly to electrostatic waves[7, 10, 13]. It has been suggested[12, 13] that it is the magnetic pressure gradient that gives rise to the electrostatic field that grows, when the FI saturates, but it has not yet been demonstrated quantitatively. This is the purpose of this paper.

We consider here the FI driven by equally dense and warm electron beams, which have a Maxwellian velocity distribution in their rest frame. This case is important, because the growth rate of the FI is highest relative to the competing mixed mode and two-stream instabilities for symmetric beams[6]. We study the FI with a particle-in-cell simulation code[16] that is based on the electromagnetic and relativistic virtual particle-mesh method[17].

The FI is modelled in a simulation reference frame, in which both beams move into opposite directions at the speed modulus $v_b = 0.3c$. We isolate the FI by selecting a 1D simulation box that is oriented orthogonally to the beam velocity vector $\mathbf{v}_b$ and we resolve all velocity components. This is an approximation for a quasi-planar boundary between filaments with an oppositely directed electron flow. They occur in warm plasmas, if the confining magnetic field cannot overcome the thermal pressure and they are characterized by planar magnetic fields[12, 14, 18]. The periodic boundary conditions of the short simulation box result in the development of only one pair of filaments. The restriction to one dimension inhibits the merging of the filaments[9] and we can analyse the relation between the electric

and magnetic fields of the quasi-stationary filaments.

Beam 1 has the mean speed $\boldsymbol{v}_{b1} = v_b\boldsymbol{z}$ and the beam 2 has $\boldsymbol{v}_{b2} = -v_b\boldsymbol{z}$. Both beams are spatially uniform and have a Maxwellian velocity distribution in their respective rest frame with a thermal speed $v_{th} = (k_bT/m_e)^{0.5}$ of $v_b/v_{th} = 18$. The 1D simulation box with its periodic boundary conditions is aligned with the $\boldsymbol{x}$-direction. We thus denote positions by the scalar x. The plasma frequency of each beam with the number density n_e is $\omega_p = (e^2n_e/m_e\epsilon_0)^{0.5}$. The total plasma frequency $\Omega_p = \sqrt{2}\omega_p$. The electric and magnetic fields are normalized to $\boldsymbol{E}_N = e\boldsymbol{E}/cm_e\Omega_p$ and $\boldsymbol{B}_N = e\boldsymbol{B}/m_e\Omega_p$ and the current to $\boldsymbol{J}_N = \boldsymbol{J}/2n_eec$. The physical position and time are normalized as $x_N = x/\lambda_s$ with the electron skin depth $\lambda_s = c/\Omega_p$ and $t_N = t\Omega_p$. We drop the indices N and $x, t, \boldsymbol{E}, \boldsymbol{B}, \boldsymbol{J}$ are specified in normalized units.

The box length $L = 0.89$ is resolved by $N_g = 500$ grid cells with the length Δ_x. The simulation time $t_S = 125$. The phase space distributions $f_1(x, \boldsymbol{p})$ of beam 1 and $f_2(x, \boldsymbol{p})$ of beam 2 are each sampled by $N_p = 6.05 \cdot 10^7$ computational particles (CPs). The total phase space density is defined as $f(x, \boldsymbol{p}) = f_1(x, \boldsymbol{p}) + f_2(x, \boldsymbol{p})$.

The electrons and their micro-currents are redistributed by the FI along x. The charge- and current-neutral plasma is transformed into one with $J_z(x) \neq 0$. The z-component of Ampere's law is in the 1D geometry $\partial_x B_y = J_z + \partial_t E_z$. A $J_z \propto \sin(kx)$ gives a $E_z \propto \sin(kx)$ and $B_y \propto -\cos(kx)$ so that E_z and B_y will have a phase shift of 90°. Figure 1 reveals this phase shift between B_y and the evanescent E_z. It also shows, that an electrostatic E_x-field grows. The $B_y(x,t)$ and the $E_x(x,t)$ oscillate in space with the wavenumbers k_1 and k_2, respectively, where $k_j = 2\pi j/L$. Both fields are spatially correlated. The comparison of E_x and B_y at $t = 56$ demonstrates that $E_x = 0$ if $B_y = 0$ or if $d_xB_y = 0$.

We determine now the relation between E_x and B_y. Let $E_B(x,t)$ be an electric field along x, which excerts the same force on an electron as the magnetic pressure gradient force does. This electric field is given in our normalization (charge $q = -1$) as $E_B(x,t) = -B_y(x,t)\, d_xB_y(x,t)$. We note that $B_y(x, t > 56)$ is quasi-stationary, while $E_x(x, t > 56)$ oscillates in time. The oscillation amplitude of $E_x(x, t > 56)$ is approximately constant and it apparently oscillates around a stationary background field. It is helpful to average the $E_x(x,t)$ and the $E_B(x,t)$ over the time interval $t_1 = 56$ to $t_2 = 125$ to give $\tilde{E}_x(x) = (t_2 - t_1)^{-1} \int_{t_1}^{t_2} E_x(x,t)\, dt$ and $\tilde{E}_B(x) = (t_2 - t_1)^{-1} \int_{t_1}^{t_2} E_B(x,t)\, dt$.

Figure 2(a) displays the $E_x(x, t = 56)$ when the FI has just saturated and reached its

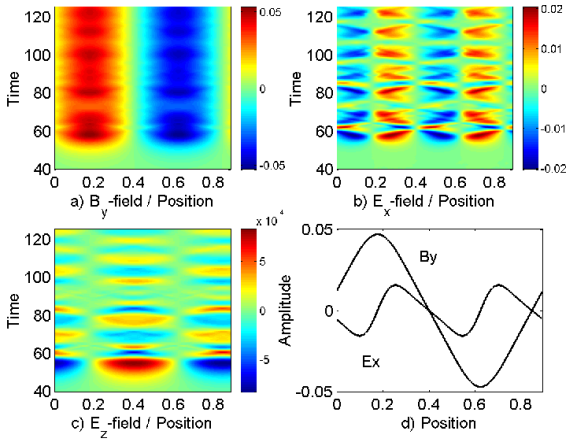

FIG. 1: (Color online) (a)-(c) show B_y, E_x and E_z. All fields are stationary in space and B_y is quasi-stationary also in time for $t > 56$. E_x oscillates in space twice as fast as B_y and both are spatially correlated for $55 < t < 125$. The phase of E_z is shifted by 90° relative to that of B_y and it is damped. The B_y, E_x fields at $t = 56$ are compared in (d).

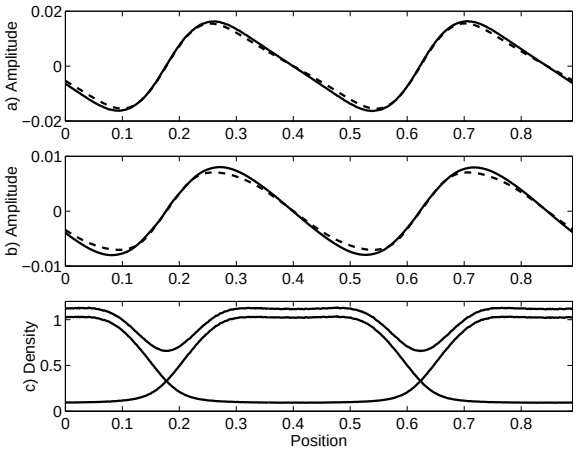

FIG. 2: (a) The $E_x(x, t = 56)$ (dashed curve) and $2E_B(x, t = 56)$ (solid curve). (b) The time-averaged $\tilde{E}_x$ (dashed curve) and $\tilde{E}_B$ (solid curve). (c) The number densities for $t = 56$, normalized to $2n_e$, of both beams separately (beam 1 is almost confined to $0.2 < x < 0.6$) and both densities added together.

peak amplitude and it compares it with $E_B(x, t = 56)$. It turns out that $E_x(x, t = 56) \approx 2E_B(x, t = 56)$. The time-averaged fields fulfill $\tilde{E}_x(x) \approx \tilde{E}_B(x)$ in Fig. 2(b). The $E_x(x, t > 56)$ oscillates in time with an amplitude $\approx \tilde{E}_B(x)$ around a stationary background field

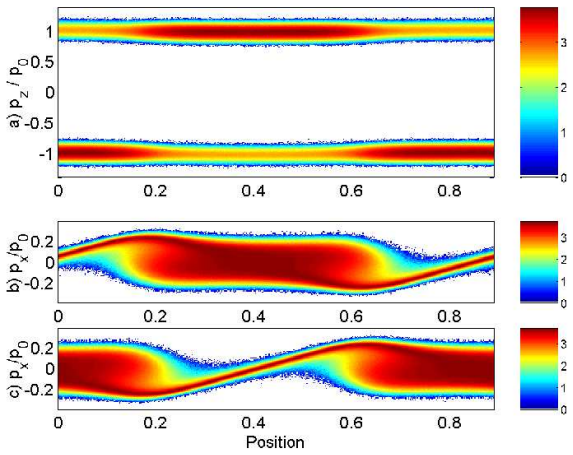

FIG. 3: (Color online) The 10-logarithmic phase space densities in units of CPs at $t = 56$: Panel (a) shows the $f(x, p_z)$ with $p_0 = m_e v_b \Gamma(v_b)$. The temperature and the mean velocity along z of the electrons are unchanged as a function of x. The density oscillates by the factor ≈ 10. The $f_1(x, p_x)$ is shown in (b) and the $f_2(x, p_x)$ in (c).

with the amplitude $\approx \tilde{E}_B(x)$. Both amplitudes add up to $2\tilde{E}_B(x)$ at $t = 56$. When the oscillatory and the background electric field have a phase shift of 180° in time, they result in a $E_x(x, t_c) \approx 0$, for example when $t_c = 75$ in Fig. 1(b).

The $E_B(x, t = 56)$ and $\tilde{E}_B(x)$ correlate well in Fig. 2(c) with the normalized number density distributions $n_{1,2}(x) = (2n_e)^{-1} \int f_{1,2}(x, \boldsymbol{p})\, d\boldsymbol{p}$ of each beam and also with the summed distribution $n_1(x) + n_2(x)$ at $t = 56$. The total density is modulated by about 30%, while that of n_1 and n_2 varies by an order of magnitude.

Figure 3 shows the electron phase space distributions $f(x, p_z)$, $f_1(x, p_x)$ and $f_2(x, p_x)$ at the time $t = 56$. The mean velocity along z of the electrons of the beams 1 (i=1) and 2 (i=2) is practically constant as a function of x. Any spatial modulation would be caused by the $\boldsymbol{E} \times \boldsymbol{B}$-force, which is given by the product of E_x and B_y in our geometry. The effects of this force are small.

The supplementary movie[19] animates in time the evolution of $f_1(x, p_x)$ and $f_1(x, p_z)$, where the color scale denotes the 10-logarithmic number of CPs. The electrons are redistributed along x but they keep their p_z almost unchanged. Their flow along x oscillates, giving a $J_x(x, t) \neq 0$. The $f_1(x, p_x)$ has a dense electron core, which rotates in the x, p_x-plane around $x = 0.4$. Two phase space vortices are convected with this rotating flow. The phase

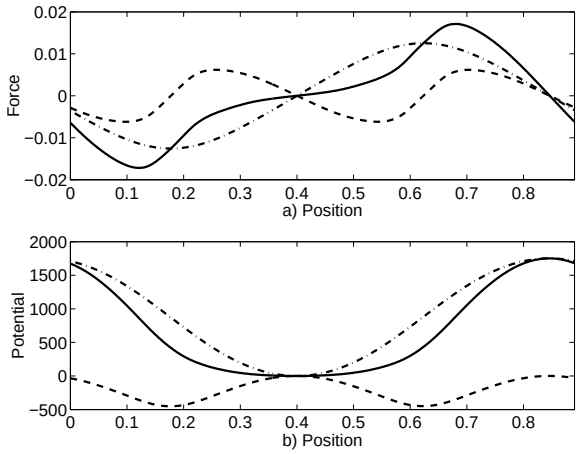

FIG. 4: The fields $\tilde{E}_j$ and the potentials $\tilde{U}_j$ averaged over $68 < t < 125$: (a) shows $\tilde{E}_x$ (dashed), $\tilde{E}_D = -v_b\tilde{B}_y$ (dash-dotted) and $\tilde{E}_T = \tilde{E}_x + \tilde{E}_D$ (solid line). Positive $\tilde{E}_j$ accelerate electrons into the negative x-direction. (b) shows the potential $\tilde{U}_x$ (dashed), $\tilde{U}_D$ (dash-dotted) and the $\tilde{U}_T$ (solid). The potential at $x = 0.4$ is the reference potential.

space motion of the electrons around the equilibrium points x_e with $E_x(x_e) = B_y(x_e) = 0$, for example $x_e = 0.4$ in the supplementary movie, reveals, that they are trapped by a potential.

We can estimate the contributions of E_x and B_y to this potential after the saturation of the FI. We average the fields $\tilde{E}_x(x) = (t_2 - t_1)^{-1} \int_{t_1}^{t_2} E_x(x,t)\, dt$ and $\tilde{B}_y(x) = (t_2 - t_1)^{-1} \int_{t_1}^{t_2} B_y(x,t)\, dt$ in time from $t_1 = 68$ to $t_2 = 125$. In what follows we consider beam 1 with $v_b > 0$. According to the supplementary movie, most of the electrons have the velocity components $v_z \approx v_b$ and $v_x \ll v_b$. The electrons retain their initial $v_y \ll v_b$, since no force component along y develops. The dominant component of the time-averaged magnetic force is thus $\tilde{F}_x = v_b\tilde{B}_y$ for $q = -1$. The time-averaged force along x is then $\tilde{F}_x = -(\tilde{E}_x + \tilde{E}_D)$ with $\tilde{E}_D = -v_b\tilde{B}_y$ and we define $\tilde{E}_T = \tilde{E}_x + \tilde{E}_D$. The time-averaged potentials $\tilde{U}_j(x) = U_{0,j} + \int_0^x \tilde{E}_j(\tilde{x}) d\tilde{x}$ with the indices $j = x, D, T$ are calculated from these fields and $U_{0,j}$ is set such that $\tilde{U}_j(x_e = 0.4) = 0$. The potentials are given in Volts.

Figure 4 displays the time-averaged fields and potentials. The $\tilde{E}_x$ destabilizes the equilibrium position $x_e = 0.4$, because the negative $\tilde{E}_x(x > x_e)$ close to x_e accelerates the electron in the positive direction and the positive $\tilde{E}_x(x < x_e)$ close to x_e in the negative direction. The $\tilde{E}_D(x \approx x_e)$ is confining the electrons around $x \approx x_e$. The $|\tilde{E}_D| > |\tilde{E}_x|$ for $x \approx x_e$ and E_T is thus a confining force. However, the electron acceleration at $x \approx x_e$ is decreased by

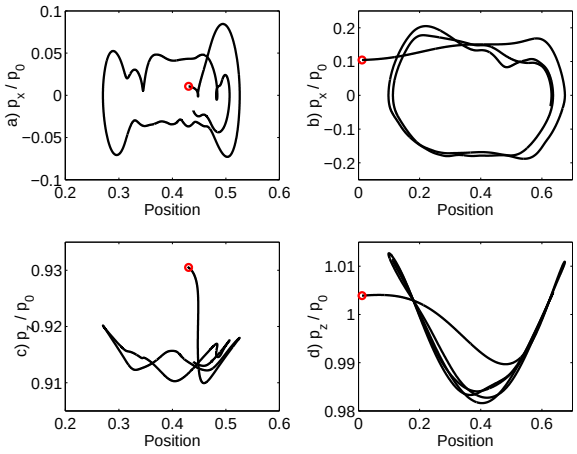

FIG. 5: The trajectories of two selected CPs: (a),(c) show the x, p_x and x, p_z diagrams of the CP 1. (b),(d) show the corresponding diagrams for the CP 2. The circle denotes the starting point of the trajectory. Both CPs follow straight paths in the x, p_x plane for $0.33 < x < 0.47$ and they are rapidly reflected outside this interval.

$\tilde{E}_x$ and increased at larger $|x - x_e|$.

The CPs of the beam 1 should follow almost straight paths close to $x_e = 0.4$ and they should be rapidly reflected for $|x - x_e| > 0.2$. The potential difference $\Delta_U = max(\tilde{U}_T) - min(\tilde{U}_T) \approx 1700$ V should trap electrons with speeds up to $\Delta_v = (2e\Delta_U/m_e)^{1/2}/v_b \approx 0.27$. This matches the momentum spread of the cool core population in Fig. 3 and in the supplementary movie. The oscillations of E_x in Fig. 1 and, thus, of the strength of the confining potential explain the periodic release of electrons from this cool core seen in the supplementary movie. The oscillatory force imposed on the electrons by $E_x(x,t)$ contributes to their heating.

Figure 5 follows the trajectories of two CPs of beam 1. The circles denote the times, when the CPs start interacting with the fields and the trajectories are followed until $t = 125$. The CP 1 has a low initial modulus of p_x and CP 2 a high one. Both CPs follow straight paths in the interval $0.33 < x < 0.47$, in which $\tilde{E}_T$ in Fig. 4 is small. The phase space path of the faster CP 2 is smoother than that of CP 1. The low speed of CP 1 implies a long crossing time of the interval with a low modulus of $\tilde{E}_T$ and the CP 1 experiences several oscillation cycles of E_x. Both CPs are reflected outside the interval $0.33 < x < 0.47$ and they remain trapped, because they can not overcome the potential difference Δ_U. Both electrons change

their v_z only by a few percent and $|v_x| < v_b/5$, which is supporting our previous assumption of a dominant and constant force $v_b\tilde{B}_y$ along x.

In summary, we have examined the saturation of the filamentation instability (FI) driven by two counter-propagating, weakly relativistic and symmetric beams of electrons. The 1D simulation box has been oriented orthogonally to $\boldsymbol{v}_b$. It can approximate the quasi-planar boundary between two filaments with oppositely directed flow, which shows up if the magnetic confinement cannot overcome the thermal pressure. This geometry is beneficial, because two of the three spatial derivatives in the Maxwell equations vanish, which separates the electrostatic and the electromagnetic fields.

We have confirmed here, that the electrostatic field, which grows during the nonlinear phase of the FI and in a 1D geometry, is driven by the magnetic pressure gradient. This has been proposed elsewhere[12, 13], but a quantitative comparison has so far been lacking. We have shown with a PIC simulation that the force imposed on an electron by the time-averaged electrostatic field $\tilde{E}_x(x)$ matches the $\tilde{E}_B(x)$, which results from the time-averaged magnetic pressure gradient force. The $E_x(x,t)$ is, however, not time-stationary, which can be explained as follows.

The FI accelerates through the magnetic pressure gradient force the electrons and a current $J_x(x,t)$ builds up. This current results in the 1D geometry with $\nabla \times \boldsymbol{B} = 0$ through the normalized equation $J_x(x,t) = -\partial_t E_x(x,t)$ in a growing $E_x(x,t)$. The initial conditions are $E_x(x,t=0) = 0$ and $J_x(x,t=0) = 0$. Any oscillatory solution for $J_x(x,t)$ and $E_x(x,t)$ implies through $J_x(x,t) = -\partial_t E_x(x,t)$ that J_x and E_x cannot simultaneously oscillate in time around their initial values. The $E_x(x,t)$ oscillates instead around its time-average, which is the background field $\tilde{E}_B(x)$. The oscillation amplitude of E_x is approximately $\tilde{E}_B(x)$. The superposed oscillatory and background field thus oscillates between $E_x(x,t_c) = 0$ at certain times t_c, fulfilling the initial condition at $t_c = 0$, and a maximum $E_x(x,t_c) = 2\tilde{E}_B(x)$.

We have confirmed previous suggestions, that the electric field force is comparable to the magnetic field force[7, 10]. We have used the time-averaged electric and magnetic forces to estimate their effects quantitatively. The electric field repels electrons at the filament centres and attracts them if they are farther away, which permits filaments to overlap and limits their peak density.

Acknowledgments: The authors acknowledge the financial support by an EPSRC Science and Innovation award, by the visiting scientist programme of the Queen's University

Belfast, by VR and by the DFG (Forschergruppe FOR1048). The HPC2N computer center has provided the computer time.

[1] T. Y. B. Yang, Y. Gallant, J. Arons, and A. B. Langdon, Phys. Fluids **5**, 3369 (1993).

[2] Y. Kazimura, J. I. Sakai, T. Neubert, and S. V. Bulanov, Astrophys. J. **498**, L183 (1998).

[3] M. Karlicky, D. H. Nickeler, and M. Barta, Astron. Astrophys. **486**, 325 (2008).

[4] M. Tabak, J. Hammer, M. E. Glinsky, W. L. Kruer, S. C. Wilks, J. Woodworth, E. M. Campbell, M. D. Perry, and R. J. Mason, Phys. Plasmas **94**, 1626 (1994).

[5] R. B. Campbell, R. Kodama, T. A. Mehlhorn, K. A. Tanaka, and D. R. Welch, Phys. Rev. Lett. **94**, 055001 (2005).

[6] A. Bret, L. Gremillet, and J. C. Bellido, Phys. Plasmas **14**, 032103 (2007).

[7] F. Califano, T. Cecchi, and C. Chiuderi, Phys. Plasmas **9**, 451 (2002).

[8] R. C. Davidson, D. A. Hammer, I. Haber, and C. E. Wagner, Phys. Fluids **15**, 317 (1972).

[9] R. Lee and M. Lampe, Phys. Rev. Lett. **31**, 1390 (1973).

[10] M. Honda, J. Meyer-ter-Vehn, and A. Pukhov, Phys. Rev. Lett. **85**, 2128 (2000).

[11] J. I. Sakai, R. Schlickeiser, and P. K. Shukla, Phys. Lett. A **330**, 384 (2004).

[12] A. Stockem, M. E. Dieckmann, and R. Schlickeiser, Plasma Phys. Controll. Fusion **50**, 025002 (2008).

[13] G. Rowlands, M. E. Dieckmann, and P. K. Shukla, New J. Phys. **9**, 247 (2007).

[14] M. E. Dieckmann, I. Lerche, P. K. Shukla, and L. O. C. Drury, New J. Phys. **9**, 10 (2007).

[15] M. V. Medvedev, M. Fiore, R. A. Fonseca, L. O. Silva, and W. B. Mori, Astrophys. J. **618**, L75 (2005).

[16] J. M. Dawson, Rev. Mod. Phys. **55**, 403 (1983).

[17] J. W. Eastwood, Comput. Phys. Commun. **64**, 252 (1991).

[18] L. O. Silva, AIP Conf. Proc. **856**, 109 (2007).

[19] See EPAPS Document No. E-PHPAEN-16- for an animation of the time-evolution of the 10-logarithmic electron phase space density. The upper part shows the projection onto the simulation direction x and the beam flow direction pz. The lower part shows the projection onto x and px. It shows the redistribution of the initially spatially uniform electrons and the formation of a current filament. The electrons gyrate in the x,px plane and form a vortex immersed in a heated population.